Describing monolayer mechanoresponse from nuclear morphology and dynamics: a computational approach

Maria Teresa Parreira
Instituto Superior Técnico
Lisbon, Portugal

ABSTRACT

Cells exhibit complex behaviour in response to mechanical stimuli, which is not yet fully understood.Studying how cells with defective mechanotransduction affect their neighbours and how this response propagates within a monolayer can help shed light on mechanisms of cellular stability and cell-cell interactions, with an impact on the study of diseases such as laminopathies or cell invasion during cancer. Here, NRK-52E cells transfected with lamin A Del50, which significantly stiffens the nucleus, were sparsely placed in a monolayer of normal, non-expressing NRK-52E cells. Through morphometric analysis and tracking, the nuclei, which play a pivotal role in mechanoresponse, were characterized and compared to a control monolayer. A method for a detailed analysis of the spatial aspect and temporal progression of the nuclear boundary was developed and used to achieve a full description of the phenotype and dynamics of the monolayers under study. Our findings reveal that cells are highly sensitive to the presence of mechanically impaired neighbours, leading to generalized loss of coordination in collective cell migration and significant changes in nuclear morphology, but without seemingly affecting the dynamics of nuclear lamina fluctuations of non-expressing cells. Interestingly, some characteristics of the behaviour of these cells appear to be dependent on the distance to a mutant cell, pointing to compensatory behaviour in response to force transmission imbalances in a monolayer.

KEYWORDS

bioimage analysis; mechanotransduction; nuclear morphometry; monolayer dynamics.

1 INTRODUCTION

In the field of cellular research, a large array of computational methods can be applied towards achieving a more complete and objective characterization of the architecture and flow of a monolayer of cells. Complex mechanisms modulate cellular stability and structure, but the mechanical balance of a monolayer can be easily affected by the presence of disrupting factors such as abnormally responsive cells[1]. Those changes in behaviour are at the origin of pathological phenomena such as laminopathies and cellular extrusion upon metastasis[2], involving force transmission imbalances within the tissues. The nucleus is known to play a pivotal role as a mechanosensor[3] and it is largely responsible for modelling cellular response to mechanical changes in the environment, but many questions remain unanswered regarding the mechanisms by which cells sense and adjust to their surroundings. How can one defective cell affect monolayer dynamics and force transmission? And, if such effects are observed, what is the range of impact? Learning the answers to these questions can boost the understanding on cellular homeostasis and disease progression.

This document is organized as follows: first, in Section 2, a brief introduction on the current knowledge on mechanotransduction mechanisms, related pathologies and implications is presented. Section 3 describes the methodology and techniques used for data acquisition and processing, specifying the different sets of features calculated and what information can be extracted. Next, Section 4 presents all the significant findings, correlating them with the biological processes underlying the conditions under study. Finally, in Section 5, a summary of the findings and suggestions on future directions of related research are presented.

2 BACKGROUND AND RELATED WORK

Mechanical stimuli in an epithelial monolayer can be propagated through the activity of myosin proteins, cell-cell adhesion and cytoskeletal remodelling[4]. The nucleus, however, is at the center of the cellular response to mechanical changes in the environment and it is often seen as a mechanosensor of high importance for normal cell behaviour[3].

The nuclear lamina is mainly composed of the lamins, V intermediate filament proteins whose functions include regulating nuclear morphology and positioning[5] and modulating nuclear stiffness[3]. Additionally, A-type lamins are involved in nuclear-cytoskeletal coupling and mechanical stress transmission through the Linker of Nucleoskeleton and Cytoskeleton (LINC) complex[6], thus creating a physical connection between the nuclear interior and the cytoskeleton. When force is transmitted to the cell, the components of the cytoskeleton reorganize and compensate for this stimulus, which can induce nuclear deformation. Cell motion and the establishment of cell polarity are also the result of a dynamic interaction between the cytoskeleton and the LINC complex, influenced by mechanosensing in cell-cell junctions and focal adhesions[7]. While the mechanisms of nuclear positioning during migration are not entirely understood, deformability of the nucleus is rate-limiting, as interphase nuclei are stiffer and more viscous than the cytoplasm[8]. Nuclear elasticity has been shown to influence migration speed, with higher nuclear stiffness being associated with smaller migration rates[9]. This can be related with the inability of the nucleus to deform. Interestingly, Graham et al.[10] describes the nucleus as a non-essential component for 2D migration and cell polarization; however, their findings reveal that regulation of cell contractility and the activation of mechanosensitivity pathways are dependent on this element of the cell.

Consequently, understanding the way by which mechanotransduction may be impaired in a cell and what is the range of this impact involves characterizing nuclear phenotype and motion. Such

disturbances can occur in laminopathies, diseases caused by mutations to the LMNA gene (which codes for lamins A and C). The specific molecular mechanisms through which some of these diseases take effect are still not fully known[3], but nuclear mechanosensing, morphology, stiffness and fragility appear to be affected[11]. Hutchinson-Gilford Progeria Syndrome (HGPS) is a laminopathy caused by the deletion of 50 amino acids near the C-terminus of the lamin A molecule, often designated del50 lamin A (Δ50LA) or progerin[12]. HGPS cells have increased levels of lamin A near the nuclear envelope, which results in nuclei that are stiffer[13], often displaying lobulations[14], which can also be observed upon introduction of Δ50LA into normal cells by transfection[13].

While the characterization of nuclei from HGPS cells has been widely described[13, 15, 16], it is not yet clear how the presence of a mechanical impaired cell - where a mutation is affecting nuclear stiffness and thus mechanoresponse - can affect the behaviour of its healthy neighbours. Philip et al.[1] demonstrated that both normal cells and cells transfected with the Δ50LA mutation increase lamin concentration in the nuclear periphery in response to shear stress. Interestingly, the same study reports that the presence of 30% of transfected cells in a normal (non-expressing) cell population is sufficient to produce an abnormal response to stress in the latter group. In line with these findings, the total lamin intensity, which reflects expression of lamins, increases more in response to prolonged shear stress in normal cells than in transfected and normal cells coexisting. Morphological nuclear changes in response to shear stress were also significantly more pronounced in the control cells than in the coexisting condition. These observations reinforce the premise that the presence of stiffer nuclei with impaired mechanoresponse has an impact on nearby normal cell response to stress, by attenuating their ability to adjust to the stimulus. It is still unclear, however, how cells in this condition behave in the absence of any external stimulus and whether the presence of sparsely placed stiffer nuclei causes sufficient force imbalance to affect nuclear functioning in normal neighbouring cells.

Here, we seek to characterize nuclear morphology, motion, and shape dynamics of normal, non-expressing (NE) NRK-52E cells in a monolayer with 5-10% of NRK-52E cells transfected with Δ50LA (mutant - M), by comparing these features with the nuclear behaviour in a monolayer of wild-type control (C) cells. We also investigate whether distance to an M cell affects nuclear behaviour. Such characterization may help shed light on cell-cell mechanosensing and on the role of the nucleus as a pivotal element in force transmission and monolayer dynamics.

3 METHODOLOGY

The following sections detail both the collection of biological data and the processing methods used for feature extraction.

3.1 Cell Culture and Transfection

NRK-52E cells were cultured in DMEM media (Thermo Fisher) supplemented with 10% FBS and imaged +2 days after plating. For the mutant nuclear variant, cells were transfected with a plasmid for Del50-LMNA-TagRFP[17] +1 day after plating, using standard lipofection according to manufacturer protocols. Two types of cell culture were prepared: one setting containing only normal NRK-52E cells; the second containing both normal, non-expressing NRK-52E cells and a small percentage of transfected, mutant NRK-52E cells, sparsely placed.

3.2 Imaging

Prior to imaging, cells were stained with 0.2μM Hoechst 33342 (1:5000 dilution) in DMEM media for 10 minutes. Subsequently, cells were washed with PBS and imaged in OptiKlear imaging media (VWR). Imaging was conducted on a Leica DMI 6000B with incubation at 37°C, using a 40X 1.25 NA objective, at 3 minute intervals over the course of 1 hour, following a previously published protocol[17].

3.3 Image Analysis

A set of 10 images (each with 21 temporal frames) was collected regarding the control monolayer (C cells) and two sets (9 and 5 images, respectively) were collected for the M+NE condition. Greyscale images (Hoechst 33342 channel) were used for downstream analysis. Segmentation and tracking were performed using ImageJ[18] and Icy[19], both Java-based bioimage analysis software. Segmentation masks and centroid coordinates were obtained (see Figure 1), but only nuclei successfully segmented throughout the 21 frames were kept for analysis.

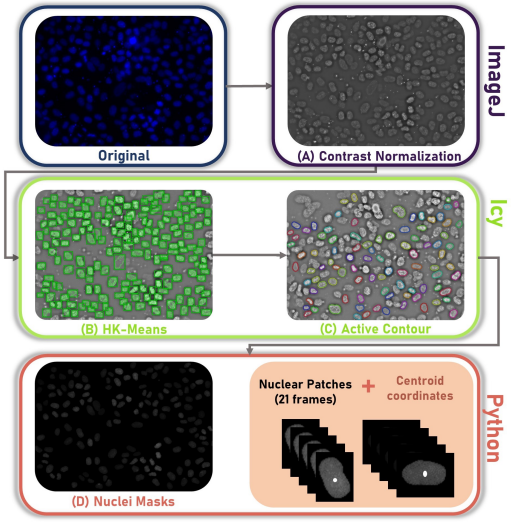

Figure 1: Overview of image processing methods used to obtain the intensity masks of each nucleus. A preprocessing step on *ImageJ* includes contrast normalization of the image stack (A), which is then input to *Icy*, where the remaining preprocessing takes place. Initial segmentation is achieved by the use of a HK-means method (B)[20], which serves as reference for the application of an Active Contour plug-in[21], accomplishing accurate segmentation and tracking of nuclei across the 21 frames (C). Finally, the region outside of the nuclei masks is zeroed and an image stack containing only the nuclei of interest is obtained, which is used for processing and feature extraction.

The process was automatized in order to reduce bias, and manual intervention was needed only for exclusion of faulty segmentation.

Furthermore, all NE nuclei with a distance to the limits of the frame inferior to 50 µm were excluded, in order to guarantee that a distance-dependent analysis was not affected by out-of-frame M nuclei.

3.4 Feature Extraction

Data was processed using python. Three main sets of features were calculated, regarding nuclear morphometric analysis, nuclear motion and detailed nuclear boundary progression (Table 1, 2 and 3).

Table 1: Nuclear motion features calculated for each nucleus.

Feature	Formula
Absolute Orientation Variation (rad/min)	$\Delta_\phi = \frac{1}{\Delta t}\frac{\sum_n^{N-1}\lvert\phi_{n+1}-\phi_n\rvert}{(N-1)}$
Direction Variation (rad/min)	$\Delta_\psi = \frac{1}{\Delta t}\frac{\sum_n^{N-2}(\psi_{n+1}-\psi_n)}{(N-2)}$
Mean Step Displacement (µm/min)	$v = \frac{1}{\Delta t}\frac{\sum_n^{N-1}\sqrt{(x_{n+1}-x_n)^2+(y_{n+1}-y_n)^2}}{(N-1)}$
Total Distance (µm)	$D_T = \sum_n^{N-1}\sqrt{(x_{n+1}-x_n)^2+(y_{n+1}-y_n)^2}$
Net Displacement(µm)	$D_N = \sqrt{(x_N-x_1)^2+(y_N-y_1)^2}$
Migration Efficiency	$\eta_D = \frac{D_N}{D_T}$

N - total number of frames; Δ_t - time (in min) between frames; ϕ_n - orientation on frame n (rad); x_n, y_n - coordinates of the nucleus centroid on frame n; ψ_n – direction of trajectory, defined as the angle between position on frame n and position on frame $n+1$ (rad).

Table 2: Morphological features calculated for each nucleus. The convex hull corresponds to the smallest convex polygon that encloses the region of interest.

Feature	Formula
Area	$A = \sum_i b_i$
Perimeter	$P = \sum_i c_i$
Aspect Ratio	$AR = \frac{mAL}{MAL}$
Eccentricity	$E = \frac{FD}{MAL}$
Circularity	$C = \frac{4\times\pi\times A}{P^2}$
Roundness	$R = \frac{4\times A}{\pi\times MAL^2}$
Smoothness	$S_P = \frac{P_C}{P}$
Solidity	$S_A = \frac{A}{A_C}$

b_i, c_i - value of pixel i in nucleus (resp. contour) binary mask; mAL, MAL, FD – Minor (resp. Major) Axis Length/ Focal Distance of the ellipse that has the same normalized second central moments as the region; P_c, A_c – Perimeter (resp. Area) of convex hull.

Nuclear morphometric features make use of segmentation masks and nuclear motion uses centroid coordinates to track for translation. To obtain data on the progression of the nuclear boundary, the contour of each nucleus was obtained and transformed into polar coordinates (ρ, θ), according to distance to the nuclear centroid, for each time frame. This corrects contours for translation (Figure 2 I a)).

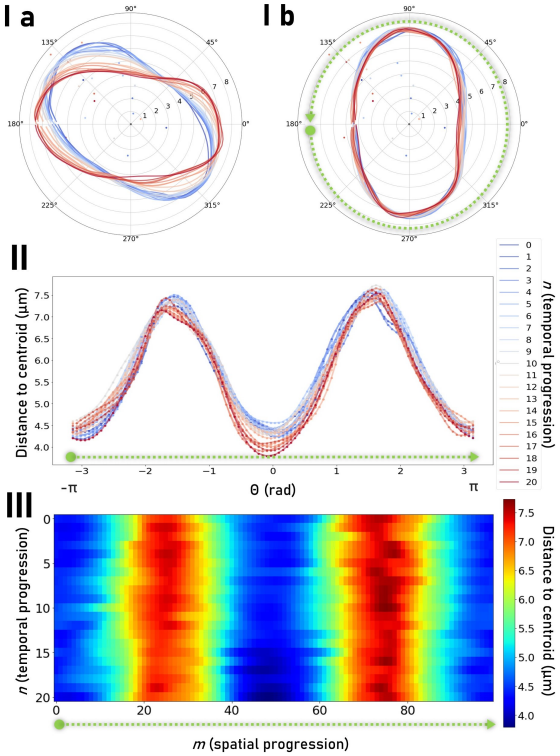

Figure 2: Data processing for numerical contour feature extraction. I) Polar representation of nuclear boundaries. Each curve corresponds to the boundary in one frame, with the centroid in $(0, 0)$. Position of the original centroid of each frame in relation to the average centroid location of the nucleus can be seen as data points of the corresponding color a) represents translation correction and b) corresponds to rotation correction. Angles in degrees, distance to centroid is in µm. II) Cubic spline interpolation results, for one nucleus. Curves represent initial contours and markers represent new contours, after interpolation, defined by 100 datapoints. III) Matrix representation of temporal and spatial progression of the nuclear boundary, coloured according to distance to centroid. Green arrows help interpretation of matrix-like representation of the contour profile.

Then, contours are corrected for rotation, *i.e.* all the nuclei are rotated until their major axis corresponds to the vertical axis (Figure 2 I b)). In order to numerically compare the boundaries for each nucleus across time, a cubic spline interpolation was applied to the polar coordinates, and every boundary became defined by a set of 100 points, corresponding to the same values of θ (Figure 2 II)). Several features can now be calculated, regarding spatial and

temporal progression of the nuclear boundary. One can imagine this progression represented in a $N \times M$ matrix, where N represents the total number of frames in the time series (21) and M represents the total number of points in the boundary (100) (Figure 2 III)). Contour magnitude is represented as numbers in the matrix. Analysing row-wise gives spatial progression or contour "static" regularity - how distance to the centroid varies for different values of θ. Column-wise analysis will provide information on temporal progression or contour "dynamic" regularity - for the same θ, how distance to centroid evolves over time. A completely homogeneous matrix, for instance, would represent a perfectly circular nucleus which is absolutely rigid, meaning its boundary does not change over time. Table 3 contains the formulas used to quantify boundary aspect and fluctuations, with analogous sets of features for spatial and temporal progression. These features are further illustrated in Figure 3.

Table 3: Contour-based features calculated for each nucleus. $r_{m,n}$ is the contour value, or distance to the centroid (ρ), for boundary position m at time n (in µm).

Feature	Formula
Contour Range	$R_s = \frac{1}{N}\sum_n^N \frac{r_{max,n} - r_{min,n}}{r_{max,n}}$
Contour Amplitude	$\Delta_s = \frac{1}{N \times (M-1)}\sum_n^N \sum_m^{M-1} \lvert\frac{r_{m+1,n} - r_{m,n}}{r_{m,n}}\rvert$
Contour Abruptness	$S_a = \frac{1}{N}\sum_n^N \max \lvert\frac{r_{m+1,n} - r_{m,n}}{r_{m,n}}\rvert, m \in [1, M-1]$
Temporal Contour Range	$R_t = \frac{1}{M}\sum_m^M \frac{r_{m,max} - r_{m,min}}{r_{m,max}}$
Temporal Contour Amplitude	$\Delta_t = \frac{1}{M \times (N-1)}\sum_m^M \sum_n^{N-1} \lvert\frac{r_{m,n+1} - r_{m,n}}{r_{m,n}}\rvert$
Temporal Contour Abruptness	$T_a = \frac{1}{M}\sum_m^M \max \lvert\frac{r_{m,n+1} - r_{m,n}}{r_{m,n}}\rvert, n \in [1, N-1]$

M – total number of points in spatial boundary (100); $r_{max,n}$,$r_{min,n}$ - maximum (resp. minimum) radius across boundary for timeframe n; $r_{m,max}$,$r_{m,min}$ - maximum (resp. minimum) radius in each boundary m, across time.

At this point, an additional, automatic step of segmentation verification can take place. Considering the *temporal* amplitude of each boundary of each nucleus, one can relate abnormally high values of amplitude to incorrect segmentation rather than nuclear behaviour, as these boundary variations would be outside of physiological ranges expected in either of the conditions analysed. To the best of our knowledge, the physiological values of nuclear boundary variation have not been published, so an empirical approach was adopted. Calculating the maximum value of temporal amplitude for each nucleus, the obtained distribution is heavily skewed to the right. As such, an upper limit for outlier detection (UL) was defined as can be seen below (Equation (1)):

$$UL = Q3 + 1.5e^{3MC}IQR \quad (1)$$

where MC corresponds to the medcouple, often used to measure skewness, $Q3$ is the third quartile and IQR is the interquartile range[22]. Abnormally segmented nuclei were detected if their temporal variation across the boundary crossed the UL value in more than 5% of the boundary extension. These nuclei were excluded from the analysis, providing a method of segmentation verification which is automatic.

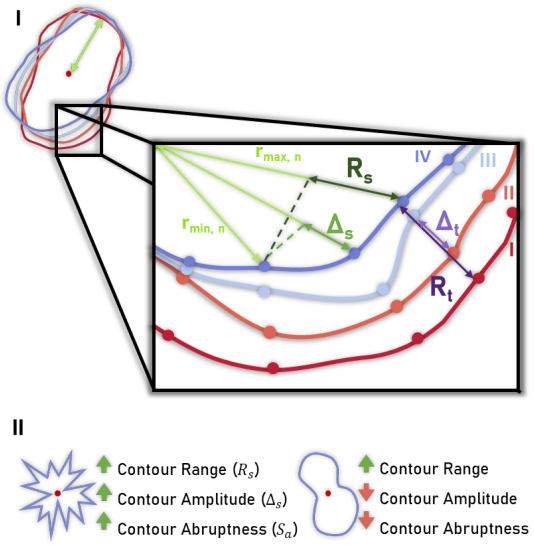

Figure 3: I) Simplified representation of contour-based features from Table 3, for a nucleus with 4 time frames (I-IV). Centroid in dark red. Δ_s is the difference in radius between subsequent points of the nuclear boundary. The maximum difference for one time frame is S_a. R_s is the difference between maximum and minimum radii. Temporal analysis concerns one boundary point across time. Δ_t is the difference between subsequent frames. The maximum Δ_s corresponds to S_s. R_t is analogous to R_s but across time. Note that features used in the analysis are averages across time or space and are normalized, unlike what is shown here. II) Illustration of nuclear aspect for different values of spatial features.

3.5 Distance-dependent analysis

For the distance-dependent analysis, each NE nucleus was characterized by the minimum euclidean distance between its centroid and the centroid of an M nucleus in-frame (see Figure 4).

A 40 µm radius difference was used to separate the group, as this guaranteed a minimum of 50 NE nuclei per distance-group per preparation. Group are named according to cell type + maximum nuclear distance, *i.e.* NE40 represents NE nuclei which are less than 40 µm apart from an M nucleus, NE80 contains nuclei which are between 40-80 µm and NE160+ includes all nuclei whose distance to an M nucleus is superior to 160 µm.

3.6 Statistical Analysis

Confidence intervals for motion and morphological features are calculated as $CI = Z\frac{\sigma}{\sqrt{n}}$, where n is the number of observations, $\overline{X}$ is the mean, σ is the standard deviation and Z is the Z-score value for the confidence level pretended[23]. A 95% CI was used ($Z = 1.96$). All groups under study had $n > 30$ except for the mutant cells ($n = 20$, although for the morphological feature analysis - Table 2 - all 21 frames of all nuclei were considered independent

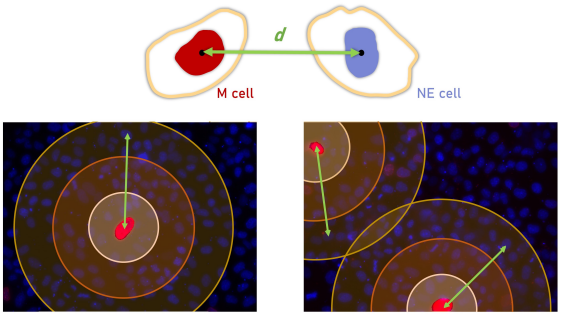

Figure 4: Illustration of group division in distance-dependent analysis. Top: schematic representation of how distance (d) between an M nucleus (red) and an NE nucleus (blue) is calculated. Bottom: nuclei within each coloured ring are part of a group characterized by a distance to an M nuclei between l_{min} and l_{max} of that ring. Where rings overlap, nuclei are attributed to group that is closer to an M nucleus. Rings are not to scale.

samples, thus for M nuclei $n = 420$). As such, under the Central Limit Theorem, normal distribution of values was assumed and statistical significance was assessed using a two-tailed unpaired t-test, without assumption of equal variance. P-values are represented using the standard scale ($ns - p > 0.05, *p \leq 0.05, **p \leq 0.01, ***p \leq 0.001, **** p \leq 0.0001$).

4 RESULTS AND DISCUSSION

The following sections present results from each different set of features calculated, which reflect dependent phenomena (*e.g.* efficient cell movement requires nuclear motion and change in shape[7]). While causality is difficult to assess, the discussion will contemplate an overview of the phenotypic differences and how they could be correlated.

4.1 Collective cell migration is less efficient in the M+NE monolayer

Nuclear motion appears to be less coordinated in the M+NE monolayer. As a consequence, direction of movement is less homogeneous and net displacement decreases (Figure 5). Fig. 6 I) reinforces the findings that the decreased net displacement is a consequence of the presence of M cells rather than a consequence of biological or experimental variability, as this phenomenon can be observed in both M+NE monolayer preparations (labelled A and B). Finally, Fig. 6 II) shows the average coefficient of variation (CV) for net direction of motion within one image. The CV is defined as the ratio between the standard deviation and the mean value of a feature and represents how "spread" the values for that feature are. The direction of motion (angle between initial and final positions of each nucleus) of NE nuclei is less defined (the motion in that monolayer of cells is less coordinated), whereas the monolayer with only normal cells has nuclei which move in unison.

A distance-dependent analysis provides further insight into the dynamics of the monolayer and mechanical force transmission, as well as energy release (Figure 7). First, the findings already mentioned for the all-normal monolayer are confirmed. C nuclei move

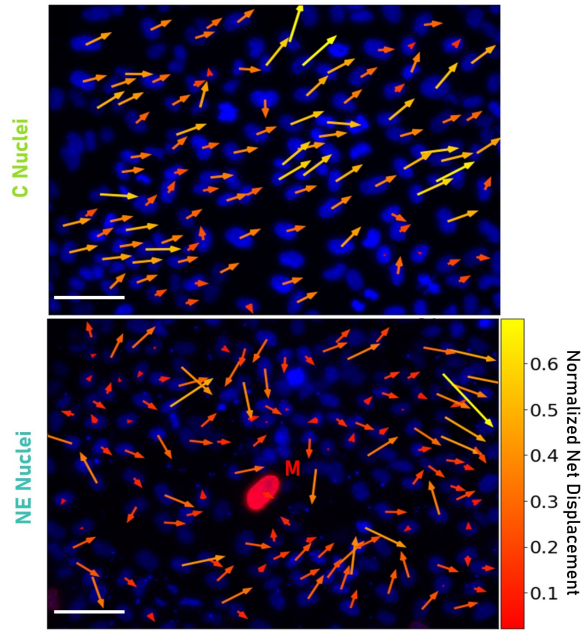

Figure 5: Monolayer dynamics are affected by the presence of M cells. A monolayer of normal cells (top) and a monolayer with normal cells (blue) and one Δ50LA cell (red) (bottom) are represented. Arrows are coloured and have a magnitude in proportion to normalized net displacement. Direction of arrows is determined by direction of net displacement vector. Bars represent 50µm. Net displacement was normalized to the maximum value of the feature.

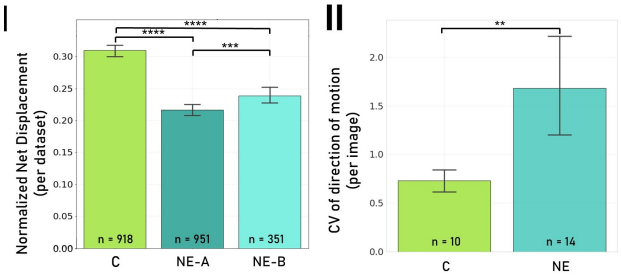

Figure 6: The differences in nuclear motion are persistent among different preparations. I) Net displacement is lower for both preparations of the M+NE monolayer, when compared to the control monolayer. II) Direction of migration is less homogeneous in the M+NE nuclei than the C monolayer. Net displacement was normalized to the maximum value of the feature. Unpaired two-tailed t-test: $** p \leq 0.01, *** p \leq 0.001, **** p \leq 0.0001$.

faster (mean step displacement represent nuclear motion velocity) and change direction significantly less than NE nuclei. As a consequence, migration efficiency is the highest amongst all groups analysed. Conversely, M cells have severely impaired nuclear movement. Their nuclei move slower than C nuclei and change direction more. Efficiency appears to be higher than NE cells, but it does not mean these cells are moving more but rather that the ratio between net displacement and total distance is superior to that of

NE nuclei, implying that, while impaired, nuclear motion is still somewhat efficiently performed. NE nuclei, in contrast, move on average faster than M nuclei but slower than C nuclei, and change direction more, which in its turn leads to lower values of migration efficiency.

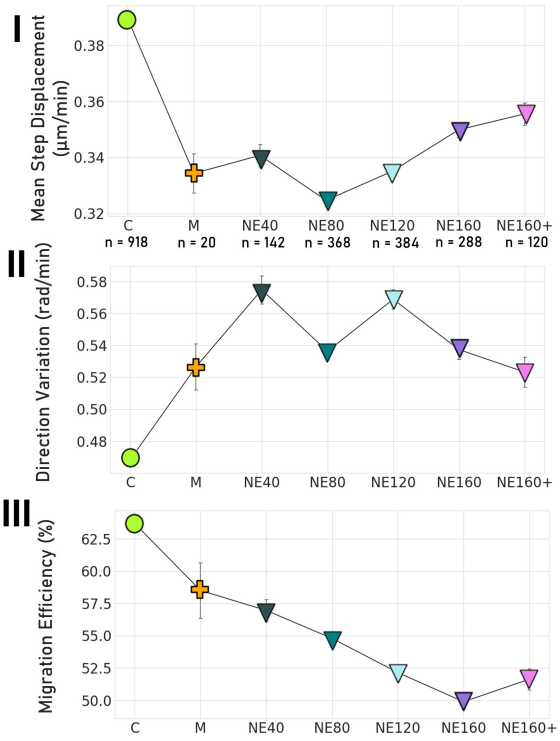

Figure 7: Distance-dependent analysis of migration features calculated. I) Mean step displacement (μm/min). II) Direction variation (rad/min) and III) Migration efficiency (%). n values indicated in I).

4.2 Morphometric analysis reveals structural differences in nuclear shape

Results regarding morphological features are presented in Figure 8. M nuclei, due to the physiological consequences of the Δ50LA mutation, are expected to have a different aspect from normal or non-expressing cells[13]. Remarkably, NE nuclei are considerably different from both M and C cells, shape-wise. While the presence of M cells does not appear to impact NE nuclear area, which is similar to that of C, NE nuclei are considerably rounder (less eccentric) than both M and C nuclei. They are less concave than M nuclei (lower solidity), indicating that boundary irregularities may occur less or have smaller amplitude.

4.3 Nuclear boundary analysis confirms morphological phenomena

With the polar representation of the nuclear boundary, further insight may be provided into the average morphological characteristics of the nuclei of each group. Figure 9 displays a distance-dependent analysis of contour-based features which reflects spatial

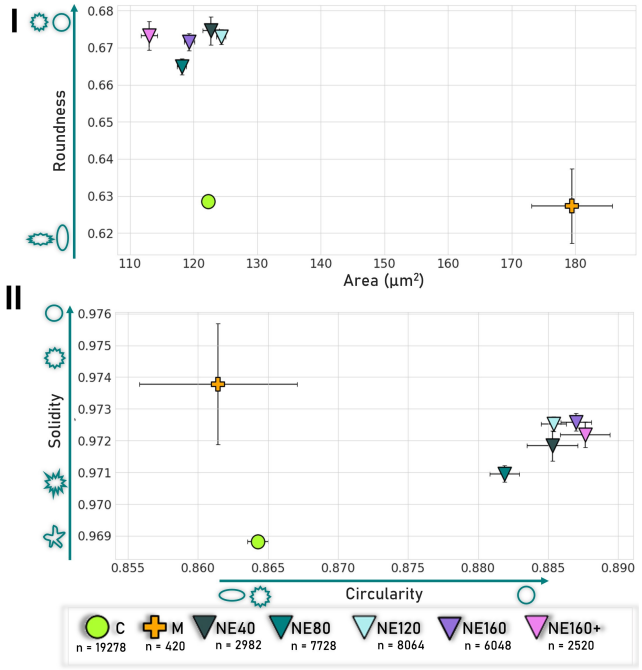

Figure 8: Distance-dependent analysis of static morphology features calculated. I) x-axis: Area (μm^2); y-axis: Roundness. II) x-axis: Circularity; y-axis: Solidity. Blue arrows and icons illustrate shape differences according to the value of that features.

progression of the contour *i.e.* a detailed analysis from a static perspective.

Contour amplitude provides a sense of mean spatial progression of the nuclear boundary. Very abrupt contours will have high values of contour amplitude. Contour abruptness relates to contour amplitude, but it is defined by the maximum (not the average) normalized Euclidean distances between subsequent points of the nucleus boundary.

Boundary irregularities seem to occur in larger amplitudes in C nuclei, when compared to both M and NE nuclei (Figure 9 I)). It is of note the growing tendency which can be observed in contour amplitude for the NE nuclei in a distance-dependent perspective, indicating that this particular effect of contour smoothing may decrease as distance to a mutant cell increases. Contour abruptness (Figure 9 II)) is smaller for NE nuclei, confirming that, indeed, these nuclei are smoother. M nuclei will not be commented due to the high heterogeneity of their phenotype regarding this feature.

Figure 9 III) roughly illustrates the findings enumerated above. It depicts a representation of the *average nuclear shape*, by taking the time-average radii for each of the 100 contour points, for all the nuclei within the population of the groups under study (C, M, NE); of course, due to the large number of cells included in the analysis, much contour detail is lost. In any case, while the area of C and NE nuclei is similar and smaller than that of M nuclei, NE nuclei do appear to be rounder than C nuclei. Note that, from the right figure in III), the representation of the time-averaged contour of all the M nuclei depicts one nucleus which is much larger than

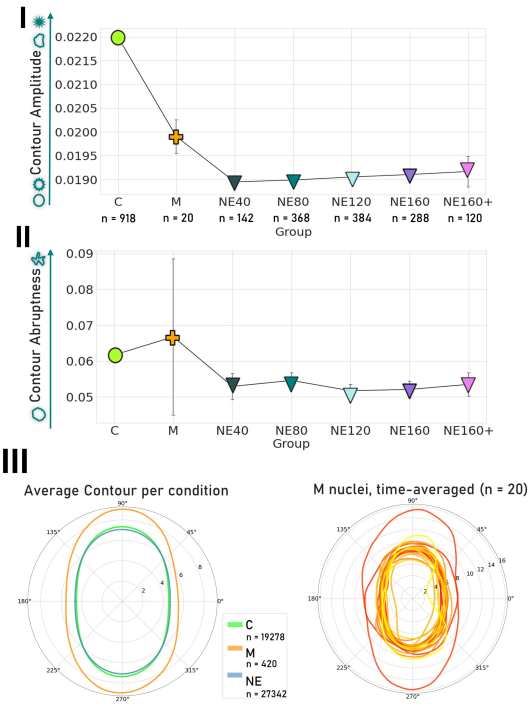

Figure 9: Distance-dependent analysis of static contour-based features calculated. I) Contour amplitude. II) Contour Abruptness. III) Polar representation of the mean contour of each group (left) and of the time-averaged contour of each of the M nuclei (right). Different nuclei represented in curves in different shades of orange. Distances to the centroid in μm.

the remaining nuclei and very eccentric, which may be biasing the characterization of this group described above.

4.4 Nuclear boundary fluctuations not affected by the presence of mechanical defects in the monolayer

Membrane fluctuations have been shown to reflect mechanical properties of cellular components and many methods have been developed with such purpose[24]. The results shown above hint that both morphology and migration of NE cells are affected by the presence of mutant, stiffer cells in the monolayer. A further insight could be provided by investigating if the nuclear membrane fluctuations which determine shape alterations are affected as well, which could reveal whether the flexibility of the nuclear envelope is maintained in NE nuclei or if these nuclei become unable to adjust to mechanical stimuli.

Figure 10 I) and II) shows that, as expected due to prior knowledge on the properties of HGPS cells[13], M nuclei have impaired morphological dynamics when compared to C cells, with significantly smaller amplitudes of temporal variation (*i.e.* due to the stiffness of their boundary, the "speed" by which the boundary changes is much smaller). Contrastingly, NE and C cells have very similar nuclear dynamics. Temporal abruptness (maximum radius variation from one frame to the other, or *how abruptly* the boundary can change) is not significantly different between both groups, indicating that the boundary stiffness is not altered in NE cells, and temporal contour amplitude (average radius variation between subsequent frames, or *how* the boundary fluctuates *on average*), while slightly inferior, is very close in average value.

The features shown reflect nuclear boundary averaged across time, but also across the boundary. A different analysis of nuclear dynamics can be performed without averaging temporal boundary variation across the spatial dimension, but rather only across time. For that, two metrics were defined, which are just variations of the calculation of temporal contour amplitude Δ_t (Table 3), but are a function of the spatial boundary m.

Relative temporal variation is calculated in a very similar way to the Δ_t, but it is not averaged across the boundary (Equation (2)):

$$\Delta_{t,rel}(m) = \frac{1}{N-1}\sum_{n}^{N-1} \left|\frac{r_{m,n+1} - r_{m,n}}{r_{m,n}}\right| \tag{2}$$

where n is one frame of $N = 21$ total frames, m is one boundary point of $M = 100$ boundary points, and $r_{m,n}$ is the distance to the nuclear centroid at that point (μm). Normalization, here, is necessary due to differences in area in different groups (Figure 8 I)). To get a sense of the absolute variation, one obtains the average differences in boundary radius over time, in μm (Equation (3)).

$$\Delta_{t,abs}(m) = \frac{1}{N-1}\sum_{n}^{N-1} |r_{m,n+1} - r_{m,n}| \quad [\mu m] \tag{3}$$

For each nucleus, $\Delta_{t,rel}(m)$ and $\Delta_{t,abs}(m)$ are fully characterized by 100 datapoints (length of nuclear boundary). From this, one can obtain Figure 10 III) and IV), which reflect temporal progression over the spatial distribution of the boundary. Each nuclear shape represented (left to right, M, NE, C) corresponds to the average temporal variations for all nuclei of the respective group. Results as represented in oval shape to facilitate interpretation. Refer to Figure 2 for an illustration of nuclear boundary alignment.

Figure 10 III) indicates that the range of boundary variation is much smaller in M cells but similar in magnitude between C and NE nuclei. Furthermore, M nuclei have a much more heterogeneous distribution of nuclear membrane fluctuations. C and NE cells, however, have corresponding regions where the relative temporal variation of nuclear radius is quite homogeneous in magnitude. Note that the regions where this magnitude is higher correspond to regions where the radius is smaller (as described in Section 3, all the nuclei are aligned so that their major axis corresponds to the vertical direction; as such, the minor axis will the correspond to angles ±180° and 0°). Note that these results refer to radius variations which are *relative* to the absolute values of radii in the boundary ($\Delta r/r$). So, when r is smaller (as in the minor axis), the observed higher magnitudes of $\Delta_{t,rel}$ may actually correspond to similar variations (Δr) across the entire boundary.

In order to verify such hypothesis, $\Delta_{t,abs}(m)$, or absolute variation of boundary, is displayed in Figure 10 IV). While M cells continue to show a very spatially heterogeneous distribution of nuclear temporal variation, it appears to be more homogeneous across the boundary in C and NE nuclei, with the exception of

boundary points near the $-\pi/2$ ($-90°$) region, where the major axis is defined. Such higher magnitudes of variation could be due to nuclear motion, with the major axis corresponding to the leading edge.

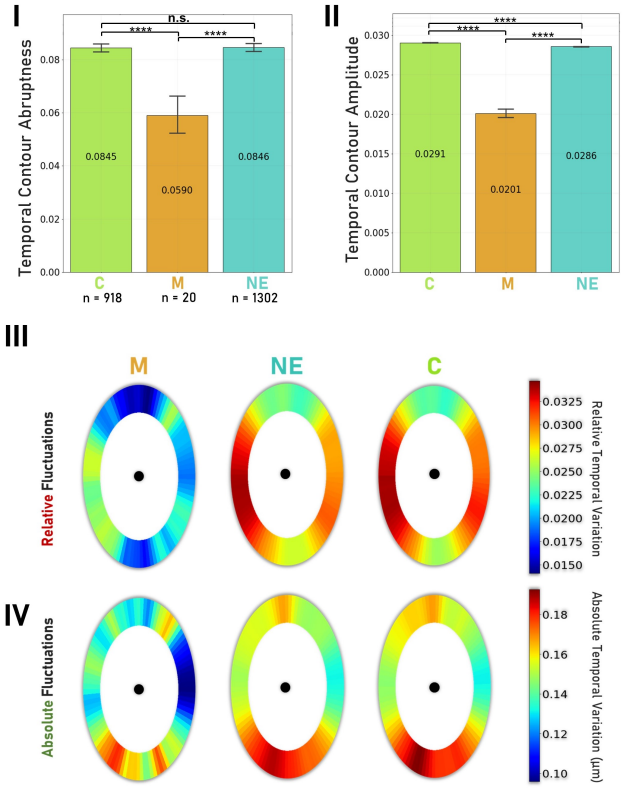

Figure 10: Group-based analysis of nuclear contour dynamics. I) Temporal contour abruptness. II) Temporal Contour Amplitude. Average value displayed on the bar. III) Average relative temporal variation, for different nuclei groups. Boundary points represented as oval shape. Magnitude (colour) reflects relative temporal variation. IV) Average absolute temporal variation (in µm), for different nuclei groups. Unpaired two-tailed t-test: $n.s. - p > 0.05; ****p \leq 0.0001$.

Another interesting analysis of nuclear boundary dynamics, though less detailed, can be performed by investigating how the numerical features calculated regarding nuclear morphology are changing over time. So, for feature F, feature variation is calculated as (Equation (4)):

$$\Delta_F(\%) = \frac{1}{N-1}\sum_{n}^{N-1} \left|\frac{F_{n+1} - F_n}{F_n}\right| \times 100 \tag{4}$$

Figure 11 allows for a distance-dependent analysis of feature variation. The heterogeneity in behaviour between different groups occurs in this case as well. In NE cells, area (I) appears to change less in the proximity of an M cell, although C nuclei-like variations can be seen as distance to a mutant cell increases.

Circularity (III), which relates shape and area-to-perimeter ratio, varies in a similar way in both C nuclei and all the groups of NE nuclei. When comparing these results with those for smoothness (II), which measures perimeter irregularities, one can see that the trend observed for NE distance-dependent groups (increase followed by decrease in variation) is opposite to that of area (decrease followed by increase in variation). Because circularity relates these two variables, this could explain why the variations in circularity are so similar for C and NE nuclei across all the different subgroups. Again, what has been described points to a distance-dependent *compensatory dynamic behaviour* in NE cells. M nuclei, has would be expected, display inferior levels of variation of morphological indicators, due to the stiffness of the boundary.

Note that Figure 10 refers to the details of the dynamics and boundary mechanics by which nuclear shape is changing, but it does not reflect the net changes in nuclear morphology. Figure 11 complements this analysis by giving an overview of how these dynamics are affecting the overall shape of the nuclei.

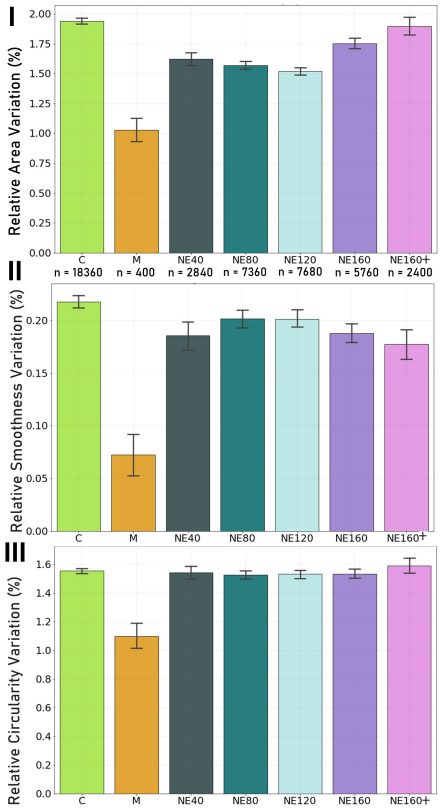

Figure 11: Distance-dependent analysis of dynamics of morphological features, in percentage of relative variation. I) Area. II) Smoothness. III) Circularity.

4.5 Discussion

A summary of the findings in this work is presented in Table 4. Regarding nuclear morphology, NE nuclei are similar in size but more round and smooth than C nuclei.

Data for M nuclei, both due to their small sample size and to their heterogeneous appearance, were included in the analysis but interpreted carefully. Overall, M nuclei analysed in the present study were larger, with similar shape to that of C nuclei (but more

Table 4: Summary of findings for C and NE nuclei (rows) for each of the feature sets analysed (columns). Trends that mention *distance* refer to observed values of that feature for different subgroups with increasing distance to a mutant cell.

Nuclei \ Feature	Nuclear Morphology	Nuclear Lamina Fluctuations	Nuclear Motion
C	• Elongated • Rough boundary	• Flexible nuclear boundary • Establishment of "leading edge", with ↑ lamina fluctuations	• Coordinated motion (↑ speed, ↓ direction changes) • High migration efficiency
NE	• Round • Smooth boundary (↓ with distance)	• Flexibility similar to C • "Leading edge" also observed	• Uncoordinated motion (↓ speed, ↑ direction changes) • Low migration efficiency (↓ with distance)
	Distance-dependent effects in nuclear motion and fluctuations, as compensatory mechanism		

eccentric than NE nuclei) and have lamina irregularities which have higher amplitude than those of NE nuclei. Choi et al.[15] describes HGPS nuclei as smaller, more round and less solid, with a large number of small blebs. Goldman et al.[25], however, studies how the accumulation of mutant Δ50LA can influence nuclear shape and describes a decrease in circularity with increased passage number, which result from perimeter increases (due to nuclear lobulation becoming more prominent) as well as an increase in area (although less pronounced than the perimeter increase, hence the observed decrease in circularity). The phenotype described in the present study would be consistent with the accumulation of the mutant lamin, but in order to take robust conclusions regarding the nuclear shape of M cells, the number of samples should be increased.

Philip et al.[1] shows that NE nuclei are more circular than C nuclei. Such observations are in line with the findings described here. Regarding the analysis of the progression of the polar description of nuclear boundary, some interesting conclusions can be drawn. The growing trend of contour amplitude (equivalent to increasing roughness) observed for the NE subgroups indicates that this morphological adaptation of NE cells to the environment may depend on distance to a mechanically impaired cell. The values for this feature, however, are still significantly inferior to the contour amplitude of C cells, indicating that smoother nuclei are a monolayer-level implication of the insertion of defective nuclei.

Still regarding morphometric analysis, but considering the dynamics by which nuclear shape adjusts over time, NE nuclei behave in a distance-dependent manner, and either preferably change shape/aspect ratio or smoothness/perimeter, resulting in similar values of circularity variation for NE cells across the whole M+NE monolayer.

Interestingly, the mechanisms by which nuclear shape is changing over time do not appear to be affected in NE cells, while for M cells, due to increased nuclear stiffness, these nuclei are considerably less flexible. These results indicate that while NE cells adapt through various mechanisms to the mechanical imbalances caused by the presence of M cells, membrane flexibility is not affected.

Upon collective cell migration in a monolayer, the large-scale reorganization required is largely regulated by mechanisms of mechanical force sensing and response[26], where propagation of these signals taking place through cell–cell junctions[4]. Mitosis and apoptosis events may cause perturbations to the dynamics of the monolayer, but the correlation between velocity vectors is usually high, indicating that a coordinated motion takes place. As was mentioned in Section 2, the nucleus and nuclear stiffness play an important role in cell migration[7], and HGPS cells migrate deficiently, which could be attributed to a decrease in nuclear deformability, decreased actin-myosin force generation[16], or inadequate establishment of cell polarization[27]. The formation of an actin-cap has been shown to be fundamental for efficient nuclear motion[28] and in HGPS cells this component is often disorganized or absent[29], so impaired migration is to be expected.

Indeed, here, a decrease in motion velocity and coordination can be observed for the M+NE monolayer. Collective migration efficiency is significantly lower for NE nuclei, on average, and it appears to decrease with distance to the defect until a distance superior to 160μm from a mutant nucleus. This is a consequence of a lower net displacement to total distance ratio. Mean step displacement (motion velocity, a proxy for total distance) increases for a distance superior to 80 μm from a mutant nucleus, hinting that the hindering of nuclear motion may a short-range effect. However, migration efficiency does not increase because net displacement (data now shown) does not increase, as a consequence of decreased coordination in collective cell migration. This implies that while the nuclei recover mobility potential when velocity starts increasing, their motion is still be impaired due to deficient force transmission or mechanoresponse from other neighbour NE cells, which is reflected in the poor coordination.

In a coordinated monolayer, cells will tend to elongate and align along preferential directions[26]. This would explain the average morphology observed for C nuclei, with NE cells having a rounder nucleus as a potential consequence of less defined direction of motion. In any case, it appears as though there is a preferential region for nuclear boundary changes in C and NE cells (Figure 10 IV)), indicating that monolayer dynamics and collective migration are dependent on the adjustment of the major axis of the nucleus and subsequent change in diameter along that direction. Cell polarization and nuclear rearward motion are to be expected in normal cells[7], and the lack of an adequate nuclear arrangement which can be observed for M cells may be related to their reported inability to establish proper cell polarization[30].

In a stable cell monolayer, contractile and extensile forces are balanced[26]. Force imbalance may occur in normal monolayers as a consequence of misalignment points, locations with undefined local cell orientation axes (also called topological defects). For the M+NE monolayer, however, potentially due to abnormal force transmission by M cells, these sites become sources of force imbalance, thus disturbing collective cell migration in neighbouring areas.

The aforementioned study by Philip et al.[1] had observed the attenuation of response to shear stress in NE cells, but the cause of this behaviour is unclear. Curiously, lamin reorganization and upregulation in NE cells appears to be impaired to a greater degree than both control and mutant Δ50LA cells. Cell-cell signaling (gene expression is affected in HGPS cells[31]) or the alteration of the flow patterns of the monolayer (due to the connection between lamins and the cytoskeleton, which is defficient in HGPS cells[13]) could be at the origin of the findings in this and in the present work.

Overall, collective cell migration is impaired in the M+NE monolayer and trajectories are more scattered and disordered due to higher changes in direction and slightly higher rotation speeds. From the nuclear lamina fluctuations observed, it appears that NE nuclei maintain the ability to adjust to mechanical stimuli; as such, what is causing the differences in nuclear shape and motion could be related to abnormal internal force generation and transmission in the M+NE monolayer. However, due to the large number of factors which are altered in HGPS cells and due to the complexity of cell-cell interactions, it is yet unclear which are the underlying causes for the phenotype observed and what is the "chain of events" leading to the morphological and behavioural differences described above.

5 CONCLUSIONS

The work presented here provides methods for the analysis and complete description of nuclear behaviour in a monolayer. A large array of techniques for image analysis and processing were used, in an attempt to objectively quantify phenotypic differences. Tracking nuclear position and maintaining identity has allowed for a dynamic study of shape evolution and nuclear motion. Because both dimensions are interdependent - nuclear motion depends on adaptation of nuclear shape and migration depends on nuclear lamina fluctuations - a better portrait of mechanoresponse and nuclear behaviour can be obtained.

The shape of NE nuclei is rounder, which could be causing the decreased velocity or could be caused by the decreased motion coordination (*i.e.* because direction of migration varies, nuclear shape does not align with preferred directions of motion). While membrane fluctuation potential points to nuclear flexibility not being affected by the presence of M cells, previous studies[1] had noted that lamin reorganization is impaired in NE cells, which could be leading to the inhibition of nuclear eccentricity and having consequences at a migration level. Distance-dependency of some of the effects observed indicates that neighbouring cells sense a mechanical imbalance and try to compensate by exhibiting abnormal behaviour which then propagates throughout the monolayer.

The present analysis could be expanded to reveal the mechanisms underlying the phenotype observed and the extent of the influence of mechanically impaired cells - topological defects - in a monolayer. Varying the density of M cells in the monolayer could improve the understanding on the mechanisms governing the behavioural changes observed. The present work analysed a monolayer with a roughly estimated density of M cells of 10%, and this was sufficient to produce generalized differences between the M+NE and the control settings. What would be the effect of an isolated M cell, both in the behaviour of this cell and its neighbours, and what could be the range of influence? Do the values of some features scale proportionally to the density of M cells (*e.g.* would migration be further debilitated and uncoordinated, would morphology become radically different)? A more complete characterization of the cellular response of NE cells to the presence of M cells could also be achieved by staining and tracking other elements of the cell (lamins, cell membrane).

By laying a basis for the understanding on nuclear behaviour in conditions of abnormal force transmission, the present work consists of yet another step in the direction of finding the principles which govern cell and tissue biomechanics, including the complex mechanisms of cellular behaviour, sensing, and interaction of internal and external stimuli. Downstream applications may include the study of mechanisms of disease onset and dissemination, with the development of better therapeutic alternatives.

ACKNOWLEDGMENTS

The preparation and imaging of the biological data used for the present analysis were skillfully carried out by Kirill Lavrenyuk in the Dahl Lab for Subcellular Structure and Engineering, Department of Chemical Engineering, at Carnegie Mellon University, Doherty Hall. The analysis was conducted under the supervision of Profs. Kris Dahl (CMU) and João Sanches (IST).

REFERENCES

[1] J. T. Philip and K. N. Dahl, "Nuclear mechanotransduction: Response of the lamina to extracellular stress with implications in aging," *Journal of Biomechanics*, vol. 41, no. 15, pp. 3164–3170, 2008.

[2] M. H. Lee, P. H. Wu, J. R. Staunton, R. Ros, G. D. Longmore, and D. Wirtz, "Mismatch in mechanical and adhesive properties induces pulsating cancer cell migration in epithelial monolayer," *Biophysical Journal*, vol. 102, no. 12, pp. 2731–2741, 2012. [Online]. Available: http://dx.doi.org/10.1016/j.bpj.2012.05.005

[3] K. N. Dahl, A. J. Ribeiro, and J. Lammerding, "Nuclear shape, mechanics, and mechanotransduction," *Circulation Research*, vol. 102, no. 11, pp. 1307–1318, 2008.

[4] X. Serra-Picamal, V. Conte, R. Vincent, E. Anon, D. T. Tambe, E. Bazellieres, J. P. Butler, J. J. Fredberg, and X. Trepat, "Mechanical waves during tissue expansion," *Nature Physics*, vol. 8, no. 8, pp. 628–634, 2012. [Online]. Available: http://dx.doi.org/10.1038/nphys2355

[5] N. Belaadi, J. Aureille, and C. Guilluy, "Under Pressure: Mechanical Stress Management in the Nucleus," *Cells*, vol. 5, no. 2, p. 27, 2016.

[6] J. Lammerding, "Mechanics of the nucleus," *Comprehensive Physiology*, vol. 1, no. 2, pp. 783–807, 2011.

[7] F. J. Calero-Cuenca, C. S. Janota, and E. R. Gomes, "Dealing with the nucleus during cell migration," *Current Opinion in Cell Biology*, vol. 50, pp. 35–41, 2018.

[8] A. L. McGregor, C. R. Hsia, and J. Lammerding, "Squish and squeeze - the nucleus as a physical barrier during migration in confined environments," *Current Opinion in Cell Biology*, vol. 40, pp. 32–40, 2016. [Online]. Available: http://dx.doi.org/10.1016/j.ceb.2016.01.011

[9] T. Harada, J. Swift, J. Irianto, J. W. Shin, K. R. Spinler, A. Athirasala, R. Diegmiller, P. C. P. Dingal, I. L. Ivanovska, and D. E. Discher, "Nuclear lamin stiffness is a barrier to 3D migration, but softness can limit survival," *Journal of Cell Biology*, vol. 204, no. 5, pp. 669–682, 2014.

[10] D. M. Graham, T. Andersen, L. Sharek, G. Uzer, K. Rothenberg, B. D. Hoffman, J. Rubin, M. Balland, J. E. Bear, and K. Burridge, "Enucleated cells reveal differential roles of the nucleus in cell migration, polarity, and mechanotransduction," *Journal of Cell Biology*, vol. 217, no. 3, pp. 895–914, 2018.

[11] M. Stiekema, M. A. van Zandvoort, F. C. Ramaekers, and J. L. Broers, "Structural and Mechanical Aberrations of the Nuclear Lamina in Disease," *Cells*, vol. 9, no. 8, 2020.

[12] K. Piekarowicz, M. Machowska, V. Dzianisava, and R. Rzepecki, "Hutchinson-Gilford Progeria Syndrome—Current Status and Prospects for Gene Therapy Treatment," *Cells*, vol. 8, no. 2, p. 88, 2019.

[13] K. N. Dahl, P. Scaffidi, M. F. Islam, A. G. Yodh, K. L. Wilson, and T. Misteli, "Distinct structural and mechanical properties of the nuclear lamina in Hutchinson-Gilford progeria syndrome," *Proceedings of the National Academy of Sciences of the United States of America*, vol. 103, no. 27, pp. 10 271–10 276, 2006.

[14] K. Manju, B. Muralikrishna, and V. K. Parnaik, "Expression of disease-causing lamin A mutants impairs the formation of DNA repair foci," *Journal of Cell Science*, vol. 119, no. 13, pp. 2704–2714, 2006.

[15] S. Choi, W. Wang, A. J. Ribeiro, A. Kalinowski, S. Q. Gregg, P. L. Opresko, L. J. Niedernhofer, G. K. Rohde, and K. N. Dahl, "Computational image analysis of nuclear morphology associated with various nuclear-specific aging disorders," *Nucleus*, vol. 2, no. 6, pp. 570–579, 2011.

[16] E. A. Booth-Gauthier, V. Du, M. Ghibaudo, A. D. Rape, K. N. Dahl, and B. Ladoux, "Hutchinson-Gilford progeria syndrome alters nuclear shape and reduces cell motility in three dimensional model substrates," *Integrative Biology (United Kingdom)*, vol. 5, no. 3, pp. 569–577, 2013.

[17] E. A. Booth, S. T. Spagnol, T. A. Alcoser, and K. N. Dahl, "Nuclear stiffening and chromatin softening with progerin expression leads to an attenuated nuclear response to force," *Soft Matter*, vol. 11, pp. 6412–6418, 2015. [Online]. Available: http://dx.doi.org/10.1039/C5SM00521C

[18] J. Schindelin, I. Arganda-Carreras, E. Frise, V. Kaynig, M. Longair, T. Pietzsch, S. Preibisch, C. Rueden, S. Saalfeld, B. Schmid, J.-Y. Tinevez, D. White, V. Hartenstein, K. Eliceiri, P. Tomancak, and A. Cardona, "Fiji: An open-source platform for biological-image analysis," *Nature methods*, vol. 9, pp. 676–82, 06 2012.

[19] F. Chaumont, S. Dallongeville, N. Chenouard, N. Hervé, S. Pop, T. Provoost, V. Meas-Yedid, P. Pankajakshan, T. Lecomte, Y. Montagner, T. Lagache, A. Dufour, and J.-C. Olivo-Marin, "Icy: an open bioimage informatics platform for extended reproducible research," *Nature methods*, vol. 9, pp. 690–6, 07 2012.

[20] A. Dufour, V. Meas-Yedid, A. Grassart, and J.-C. Olivo-Marin, "Automated quantification of cell endocytosis using active contours and wavelets," *Proceedings - International Conference on Pattern Recognition*, no. May 2014, 2008.

[21] A. Dufour, R. Thibeaux, E. Labruyere, N. Guillen, and J. Olivo-Marin, "3-D Active Meshes: Fast Discrete Deformable Models for Cell Tracking in 3-D Time-Lapse Microscopy," *IEEE Transactions on Image Processing*, vol. 20, no. 7, pp. 1925–1937, 2011.

[22] M. Hubert and S. Van der Veeken, "Outlier detection for skewed data," *Journal of Chemometrics*, vol. 22, no. 3-4, pp. 235–246, 2008. [Online]. Available: https://onlinelibrary.wiley.com/doi/abs/10.1002/cem.1123

[23] S. M. Ross, "Chapter 7 - parameter estimation," in *Introduction to Probability and Statistics for Engineers and Scientists (Fifth Edition)*, fifth edition ed., S. M. Ross, Ed. Boston: Academic Press, 2014, pp. 235 – 296. [Online]. Available: http://www.sciencedirect.com/science/article/pii/B9780123948113500071

[24] C. Monzel and K. Sengupta, "Measuring shape fluctuations in biological membranes," *Journal of Physics D: Applied Physics*, vol. 49, no. 24, 2016.

[25] R. D. Goldman, D. K. Shumaker, M. R. Erdos, M. Eriksson, A. E. Goldman, L. B. Gordon, Y. Gruenbaum, S. Khuon, M. Mendez, R. Varga, and F. S. Collins, "Accumulation of mutant lamin A progressive changes in nuclear architecture in Hutchinson-Gilford progeria syndrome," *Proceedings of the National Academy of Sciences of the United States of America*, vol. 101, no. 24, pp. 8963–8968, 2004.

[26] T. Chen, T. B. Saw, R. M. Mege, and B. Ladoux, "Mechanical forces in cell monolayers," *Journal of Cell Science*, vol. 131, no. 24, 2018.

[27] C. Östlund, W. Chang, G. G. Gundersen, and H. J. Worman, "Pathogenic mutations in genes encoding nuclear envelope proteins and defective nucleocytoplasmic connections," *Experimental Biology and Medicine*, vol. 244, no. 15, pp. 1333–1344, 2019.

[28] D. H. Kim, S. Cho, and D. Wirtz, "Tight coupling between nucleus and cell migration through the perinuclear actin cap," *Journal of Cell Science*, vol. 127, no. 11, pp. 2528–2541, 2014.

[29] S. B. Khatau, C. M. Hale, P. J. Stewart-Hutchinson, M. S. Patel, C. L. Stewart, P. C. Searson, D. Hodzic, and D. Wirtz, "A perinuclear actin cap regulates nuclear shape," *Proceedings of the National Academy of Sciences*, vol. 106, no. 45, pp. 19 017–19 022, 2009. [Online]. Available: https://www.pnas.org/content/106/45/19017

[30] W. Chang, Y. Wang, G. W. G. Luxton, C. Östlund, H. J. Worman, and G. G. Gundersen, "Imbalanced nucleocytoskeletal connections create common polarity defects in progeria and physiological aging," *Proceedings of the National Academy of Sciences*, vol. 116, no. 9, pp. 3578–3583, 2019. [Online]. Available: https://www.pnas.org/content/116/9/3578

[31] J. Lammerding, P. C. Schulze, T. Takahashi, S. Kozlov, T. Sullivan, R. D. Kamm, C. L. Stewart, and R. T. Lee, "Lamin A/C deficiency causes defective nuclear mechanics and mechanotransduction," *Journal of Clinical Investigation*, vol. 113, no. 3, pp. 370–378, 2004.